LAWRENCE
LIVERMORE
NATIONAL
LABORATORY

LLNL-CONF-437771

Development of High Performance Vacuum Power Flow Interface For Explosive Magnetic Flux Compression Generator Experiments

D. A. Goerz, J. B. Javedani, G. E. Vogtlin, T. L. Houck, M. P. Perkins, D. B. Reisman

June 22, 2010

The 13th International on Megagauss Magnetic Field Generation and Related Topics
Suzhou, China
July 6, 2010 through July 10, 2010

Disclaimer

Development of High Performance Vacuum Power Flow Interface For Explosive Magnetic Flux Compression Generator Experiments

D. A. Goerz, J. B. Javedani, G. E. Vogtlin, T. L. Houck, M. P. Perkins, and D. B. Reisman
Lawrence Livermore National Laboratory
Livermore, CA 94550 USA
Email: <goerz1@llnl.gov>

ASTRACT

Certain types of physics experiments and material studies require operation in a vacuum environment. For material studies requiring extremely high energy density and applied pressure, magnetic flux compression generators can be utilized, and typically their performance far surpasses that of capacitor bank systems. LLNL has developed a family of advanced magnetic flux compression generators used to perform high energy density physics experiments. One of the most critical aspects of doing such HEDP experiments is coupling the very powerful flux compression generators to the loads through vacuum power flow regions. We have developed a high performance vacuum power flow interface that satisfies these experimental requirements. The techniques we employed include shaping electrodes and insulators to manage electric field enhancements, coatings on cathode surfaces to suppress electron emission, baffles in the channel to block UV, and coatings on electrode surfaces to absorb UV. In addition, we took advantage of the strong magnetic fields to inhibit flashover of the insulator surface and provide magnetic insulation in the narrow power flow channel. This paper describes the design of a low-inductance vacuum power flow channel incorporated into a coaxial FCG that can deliver 100 MA and 66 MJ to an inductive load. We describe the basic physics and engineering requirements, the design parameters, modeling and simulation results, and laboratory testing that was performed to qualify performance before successful utilization in explosive pulsed power experiments.

INTRODUCTION

At Lawrence Livermore National Laboratory we have developed a family of advanced explosively driven magnetic flux compression generators used to perform high energy density physics experiments. Our largest FCG platform is comprised of a high-gain helical generator coupled to a ring-lit coaxial generator. The advanced helical generator[1] (AHG) can produce currents of 20 MA and deliver energies of 20 MJ. The coaxial generator (CG), when coupled with the AHG, can deliver 100 MA currents and over 66 MJ energies to experimental loads. To date we have conducted four full function tests [2] (FFT) of the combined AHG-CG system while successfully performing HEDP experiments. Figure 1 shows a FFT assembly along with a cutaway drawing view of the AHG and CG devices.

The AHG consists of a 49-cm-diameter helical stator of 1-m length and a 31-cm-diameter cylindrical armature. The stator is comprised of 5 sections with 2 parallel conductors in the first two sections, then bifurcations in the coil resulting in 4, 8, and 16 parallel conductors in the last three sections. The armature is filled with 157 kg of PBXN-110 cast explosive. Further details of the construction are discussed in the published literature[1]. The AHG has a nominal inductance of 27 μH, and when seeded with a 140-kA current, can produce approximately 20 MA into the 80-nH inductance of the CG at crowbar time.

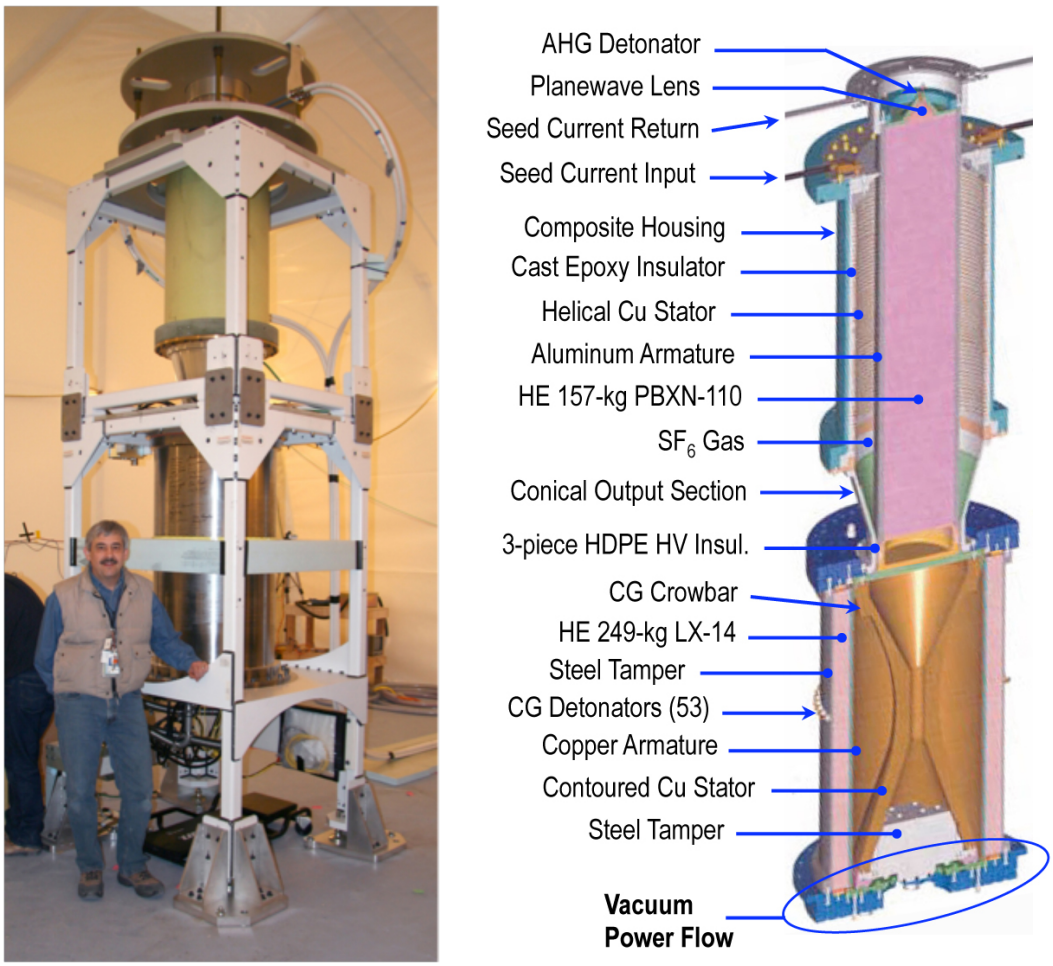

Figure 1. a) Photo of FFT assembly comprised of (top) advanced helical generator (AHG) and (bottom) ring-lit coaxial generator (CG). **b**) Cutaway view of AHG and CG components.

The ring-lit coaxial generator is based on an earlier design by Shearer at LLNL[2], with modern day improvements by Reisman et al.[3]. The CG device operates by imploding a cylindrical copper armature onto a contoured copper stator. The 50-cm diameter armature is surrounded by 249 kg of pressed and machined LX-14 explosive. On the outside of the HE, near the middle of the 130-cm long cylindrical shell, a ring of 53 detonators simultaneously initiates the explosive. Figure 2 shows the results of the hydrodynamic operation of the HE burn using ALE3D simulations[4]. The armature is squeezed inward, moving first under the waist region of the detonator ring. The deformed shape of the armature begins to resemble the contour of the stator. At the appropriate time the armature contacts the stator near the input side, which crowbars the AHG. The armature continues to move, and the shapes of the armature and contoured stator are designed to produce a fast, axially moving contact ring at a shallow angle between the armature and stator, which rapidly sweeps flux into the load, resulting in fast current rise at high energy levels.

Just producing high currents and large energies is not enough for most useful applications; delivering that energy to a load becomes the most critical aspect. In many of the HEDP

experiments and material studies of interest, operation in a vacuum environment is required. In addition, achieving extremely high energy densities requires that energy be delivered to very small volumes having correspondingly high inductances.

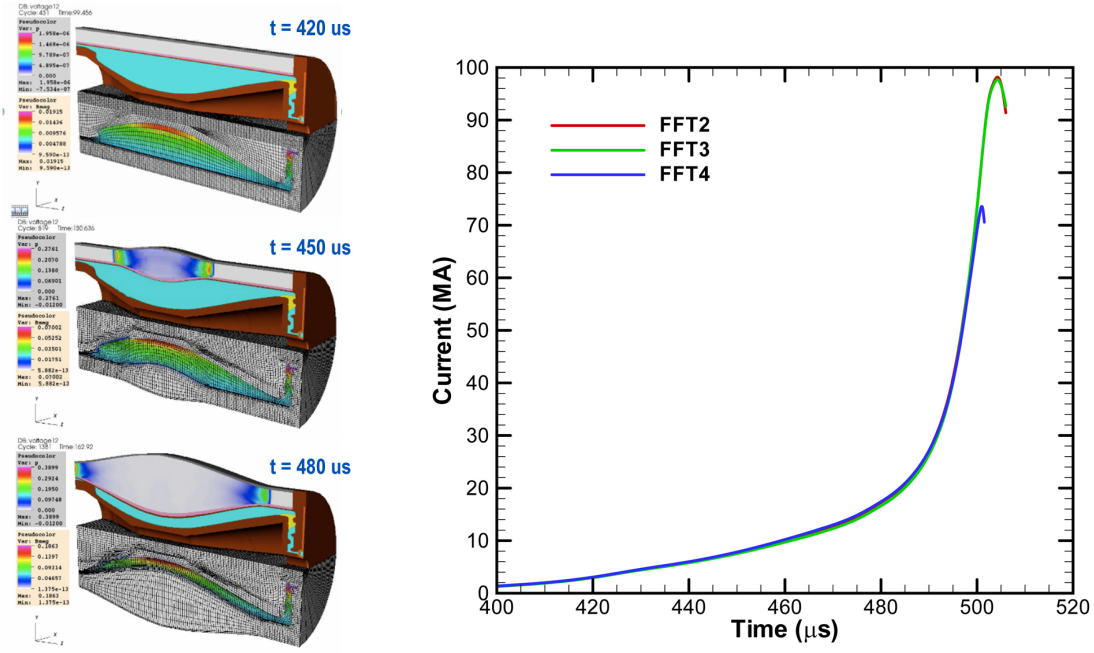

Figure 2. a) (Color) ALE3D simulation of MHD operation for ring-lit coaxial generator showing formation of armature shape matching contoured stator. **b**) (Color) Current waveforms from FFT experiments showing fast exponential rise of output current.

We have developed a high performance vacuum power flow interface that satisfies these experimental requirements for our purposes. The design we report on here has a gas-to-vacuum interface designed to withstand voltages exceeding 100 kV, and a power flow channel between the FCG output and load input having a low 5.4-nH inductance.

VACUUM INTERFACE AND POWER FLOW CHANNEL

Figure 3 shows a cross sectional view of our vacuum interface and power flow channel. We employ a solid dielectric to separate the gas-filled region of the generator from the vacuum region of the power flow channel, and to serve as a mechanical structure and electrical insulator between the anode and cathode flanges. In this figure the outermost and rightmost electrodes are of positive polarity whereas the innermost and leftmost electrodes are of negative polarity. This is determined by our selection of polarity in providing the seed current to the AHG.

We have incorporated the best engineering practices for vacuum insulators into our design; including, a positive angled between the insulator surface and cathode electrode[5], a so-called cathode bump on the electrode in close proximity to the cathode triple junction[6], a so-called anode plug embedded into the insulator in close proximity to the anode triple junction[7,8], and an anodized coating on the cathode surface to suppress electron field emission[9], particularly along the cathode bump which is in close proximity to the insulator surface.

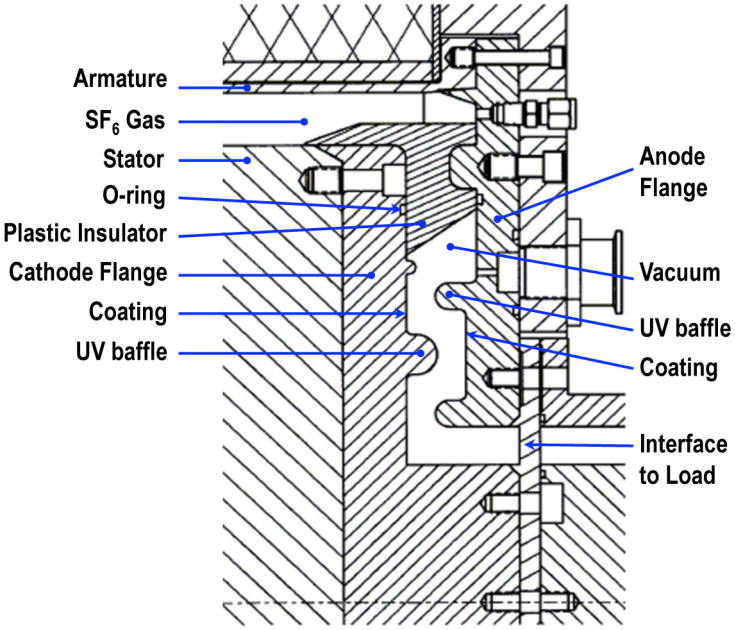

Figure 3. Cross sectional view of the vacuum interface and power flow channel. The insert shows the location with respect to the coaxial generator output.

There are three distinct regions where basic design requirements must be established and satisfied, the gas-filled region on the generator side, the body of the solid dielectric insulator, and the vacuum region along the insulator surface. These regions are depicted in Figure 4, along with a color-graded scale of field stress in each region, and equipotential lines between electrodes. We set maximum field stress levels for our design in each region based on published literature. For SF6 gas at one atmosphere pressure the level is 75 kV/cm for DC or very long pulses. For 6-mm thick solid polyethylene material the level is 190 kV/cm for 8-μs pulses[10]. For +45 degree angled insulator surface the level is 140 kV/cm for 5-μs pulses[11]. In Figure 4 the top of the color scale (red) is the set threshold value for that region. For the dimensions we choose for our insulator the field stress levels are at least a factor of two below the set threshold value, as apparent in the colored regions in Figure 4. This represents the safety factor in our design, if the applied voltage is 100 kV, as was used in the field modeling runs.

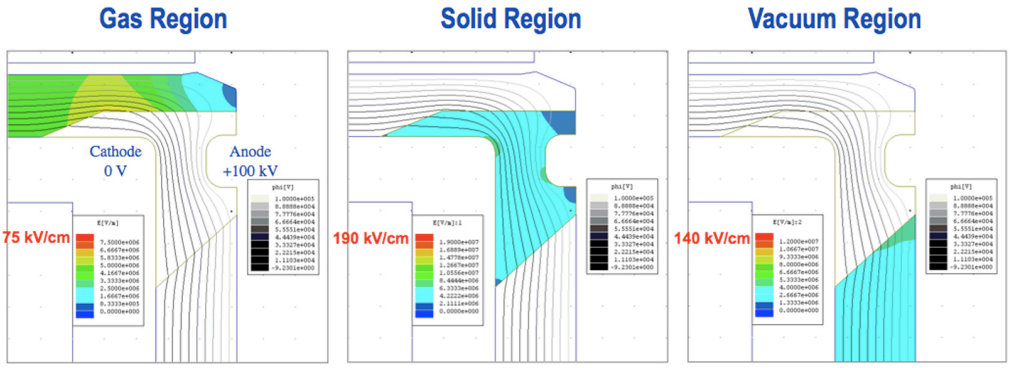

Figure 4. Electric field stress levels in gas, solid, and vacuum regions are kept below design thresholds of 75, 190, and 140 kV/cm respectively.

We have used high-density polyethylene and polystyrene as plastic insulator materials in our FFT experimental platforms. Both have worked satisfactorily; however, HPDE tends to creep more under compression, which can introduce some mechanical issues. Milton evaluated surface flashover thresholds for various other materials exposed to 5-μs HV pulses in vacuum[11]. We have evaluated mica-filled glass and machinable ceramic materials, both of which have been used in other HV vacuum insulator applications. Generally, we found that lower dielectric constant materials can withstand higher voltages before surface flashover. Work is continuing at LLNL to better understand surface flashover mechanisms and improve insulator performance[12,13,14].

The efficiency of the energy delivered by the generator to the load is strongly dependent on geometry. It is desirable to have as low of inductance as possible. Reducing the gap between electrodes in vacuum or reducing the path length between the insulator and the load are ways to obtain low inductance. Reducing the gap spacing increases electrical field stress, which can cause electron emission from the cathode. Reducing the path length between the insulator and the load provides a more direct path for UV from a load to reach the vacuum insulator surface.

We employed proven techniques to handle these problems; including, shaping electrodes and insulators to manage electric field enhancements, coatings on cathode surfaces to suppress electron emission, baffles in the channel to block UV, and coatings on electrode surfaces to absorb UV. In addition, we took advantage of the strong magnetic fields to inhibit flashover of the insulator surface and provide magnetic insulation in the narrow power flow channel.

In addition to this development effort, there were other projects underway at LLNL to investigate HV vacuum insulator flashover. We were able to utilize a HV vacuum test stand from these projects to test materials and coatings. This test stand is shown in Figure 5.

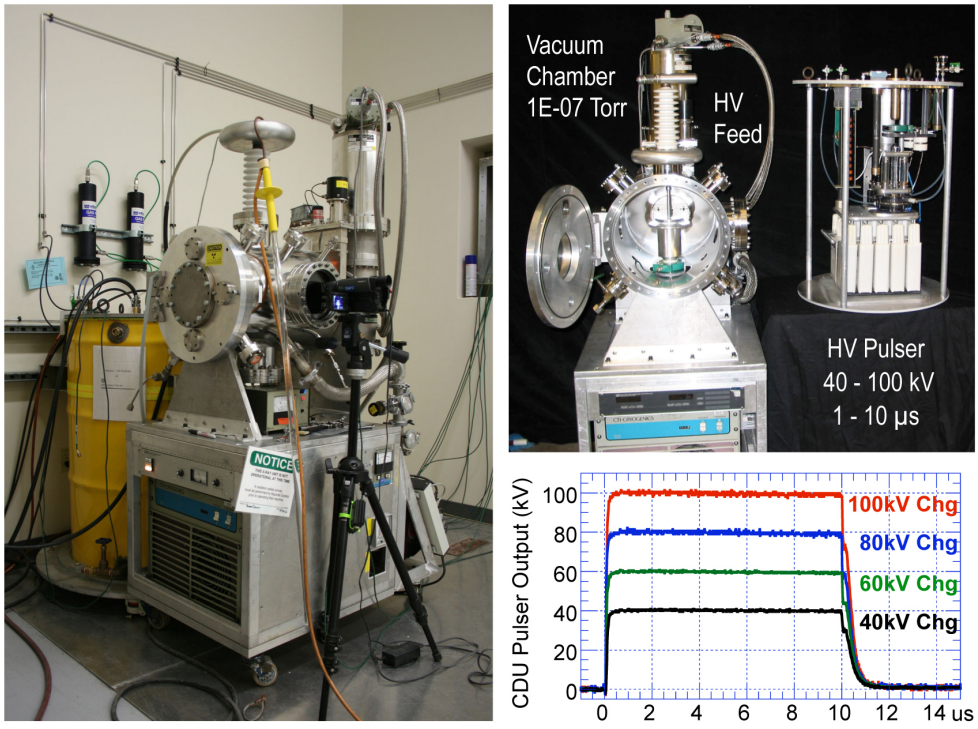

Figure 5. HV vacuum test stand in LLNL's PP Lab used to test insulator materials, shapes, and coatings. Capacitor discharge unit can produce variable pulse widths and voltages up to 100 kV.

The test stand incorporates a capacitor discharge unit that can operate up to 100 kV using spark gap switches to adjust pulse width from 1 to 10 μs or longer[15]. One of the uses of the test stand was to evaluate coatings to be applied on the cathode surface to suppress electron emission. Figure 6 shows the setup and results from a representative sample, which passed a screening test of 280 kV/cm for 15 μs.

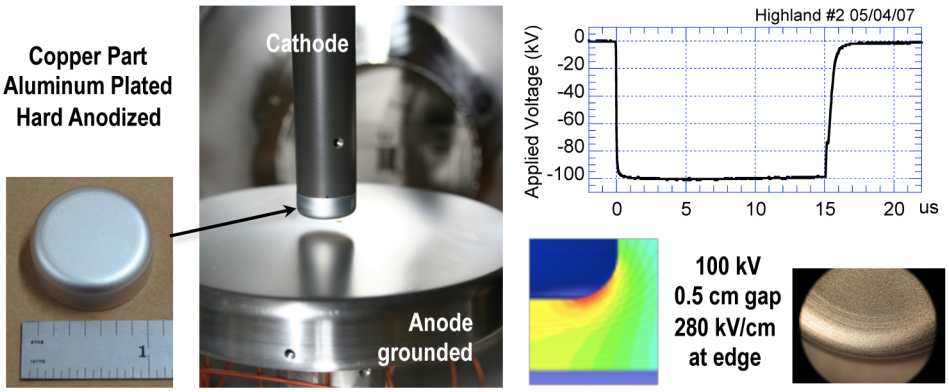

Figure 6. Coatings were tested in HV vacuum test stand to evaluate ability to suppress electron emission. The sample shown in this figure passed a test exposing to 280 kV/cm for 15 μs.

UV BAFFLES AND COATINGS

There have been many studies that show that UV illumination can induce flashover of insulators. It is believed that UV exposure causes electrons to leave the insulator surface, resulting in net positive charge that distorts the electric fields, creating suitable conditions for electrons to avalanche along the surface. Enloe, et al. did experiments to investigate and quantify photon fluence and energy levels that would induce insulator flashover[16,17]. Javedani et al. at LLNL have since performed further testing [18,19].

From the available data we established a threshold of incident UV on the insulator surface that could likely be tolerated. We designed baffles in the power flow region to block UV coming from the load, and sized them to minimize field enhancements along the cathode surface. After a preliminary analysis of how much UV would be reaching the insulator, we recognized it would be necessary to apply coatings to the surfaces to absorb significant amounts of UV.

A study was done to examine and quantify the desirable properties and select suitable coating materials. A ray-tracing code, FRED[20] was used to determine the fraction of source fluence striking the insulator. Figure 7 shows a representation of the problem and results from several case studies. Individual case runs assume different percent reflectance for electrode coatings. Case 1 shows the unity amount of UV reaching the insulator assuming the walls are 100% reflective. Case 2 shows the reduced amount of UV reaching the insulator assuming the walls are 80% reflective.

Figure 8 shows the surface charge density required to modify the electric field sufficiently to likely induce flashover. For a postulated UV fluence of 0.38 J/cm^2 from the load, and surfaces having 36% reflectivity, assuming a 0.2% efficiency of photoionization, the resulting 18.2 nC/cm^2 would appear to be enough to induce insulator flashover.

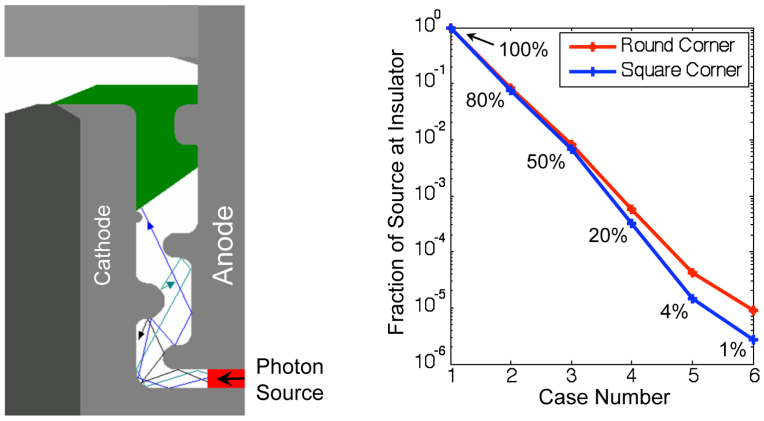

Figure 7. A ray-tracing code (FRED) is used to determine the fraction of source fluence striking the insulator. Individual case studies assume different percent reflectance for electrode coatings.

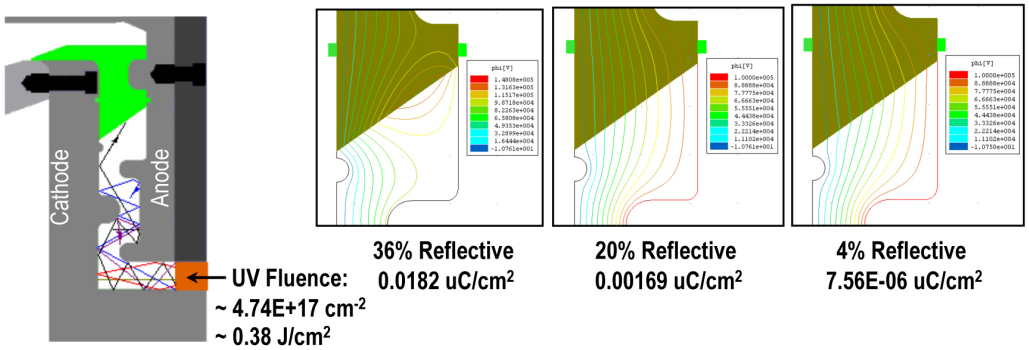

Figure 8. Field modeling showing distortion of equipotential lines resulting from charge deposition from UV illumination. With 18.2 nC/cm^2, distortion is sufficient to expect flashover.

To support our analysis we obtained reflectivity measurements on candidate coating materials. Figure 9 shows measured UV reflectance data from copper surfaces in the wavelength range from 200 to 400 nm, along with similar reflectance data from a manufacturer of special UV absorbing coatings. Whereas copper with different finishes will reflect up to 50% of the UV at these wavelengths, the Avian DS Black coating will absorb more that 98% of the incident UV.

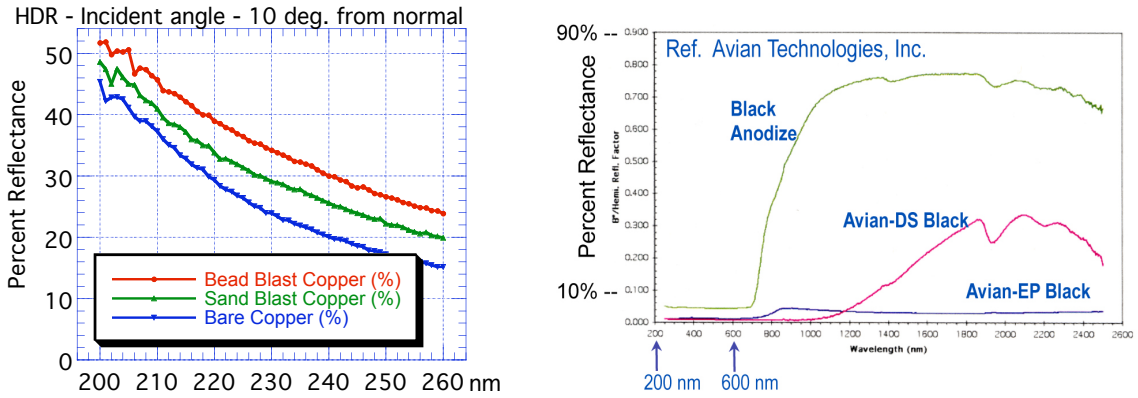

Figure 9. Measured UV reflectance data from copper surfaces and special absorbing coatings.

We obtained similar reflectivity measurements on samples of anodized aluminum as shown in Figure 10. Anodized coatings themselves are fairly good UV absorbers; however, their performance can vary significantly depending on substrate material, type of processing, and thickness of coating. Since we had already planned to rely on an anodized coating on the cathode for suppressing electron emission, we performed further analysis for selected providers.

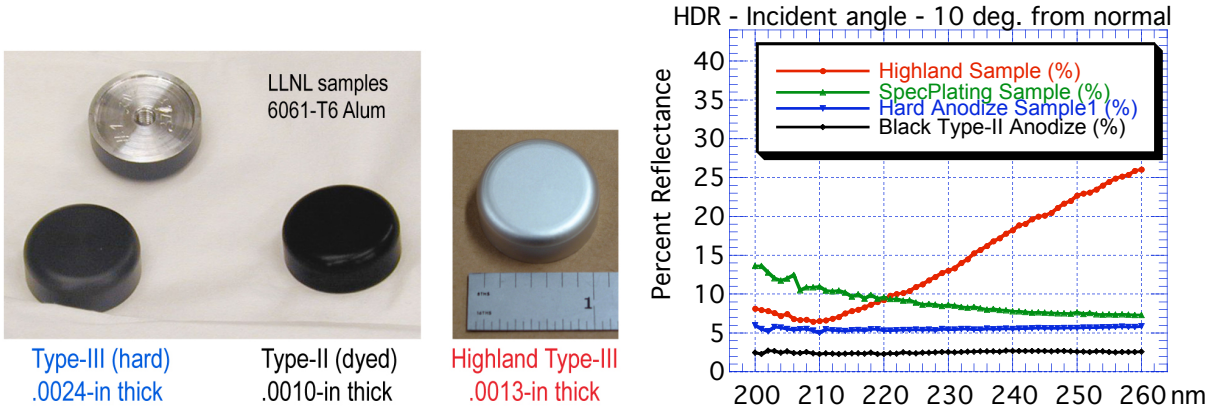

Figure 10. Measured UV reflectance data from different types of anodized aluminum

Our baseline design used Type-III anodized coating on the cathode and Avian Black-S coating on the anode. Avian Black-S is a two-part water-based urethane coating having a reflectance less than 3.5% over most of the UV-Vis-NIR spectrum. Table 1 shows the calculated fraction of source fluence striking the insulator for two different anodized coatings, assuming either specular or diffuse reflection, and either square or rounded corner at the innermost region opposite the load interface.

Table 1. Fraction of source fluence striking insulator found from ray-tracing analysis.

	Square Corner Diffuse Anal.	Round Corner Diffuse Anal.	Square Corner Specular Anal.	Round Corner Specular Anal.
Spec Plating	3E-5	7E-5	2E-4	4E-4
Highland	7E-5	1E-4	3E-4	5E-4

MAGNETIC INHIBITION OF INSULATOR FLASHOVER

All of the analysis we did for the design tradeoffs we made indicated that insulator flashover would be unlikely for our expected experimental conditions. Plus we had not yet taken into account the role of magnetic inhibition of insulator flashover. The intense magnetic field in the power flow region acts on electrons emitted from the cathode. The $E\ X\ B$ drift of electrons near the insulator is directed away from the insulator surface, thereby inhibiting the formation of an avalanche which otherwise could break down the insulator[21]. Vandevender et al. observed MFI for 45° angled insulators when $E < 2.1 \times 10^7$ B (MKS units). Based on this criteria, our insulator at r=0.18m, with a 100 kV applied potential, should experience MFI when the current

exceeds 122 kA. At the time our insulator is exposed to 100 kV the magnetic field is an order of magnitude higher than this.

As an additional check, we performed 3D particle-in-cell modeling of the insulator with 0.0182-μC/cm^2 positive charge on the insulator, corresponding to the 36% UV reflectance case. The results show that even with this much net positive charge from UV illumination, MFI keeps electron from avalanching along the insulator surface.

SUMMARY and CONCLUSION

We have developed a high performance vacuum power flow interface for our family of advanced magnetic flux compression generators. The techniques we employed include shaping electrodes and insulators to manage electric field enhancements, coatings on cathode surfaces to suppress electron emission, baffles in the channel to block UV, and coatings on electrode surfaces to absorb UV. In addition, we benefit from the strong magnetic fields that inhibit flashover of the insulator surface and provide magnetic insulation in the narrow power flow channel. The power flow interface has been field tested on four successful high energy density physics experiments.

ACKNOWLEDGEMENTS

The authors would like to acknowledge the outstanding support of associate electrical engineer Ron Speer and associate mechanical engineer Tony Ferriera along with their technical staff who performed experiments in the Pulsed Power Lab and supported field tests. This work performed under the auspices of the U.S. Department of Energy by Lawrence Livermore National Laboratory under Contract DE-AC52-07NA27344.

REFERENCES

[1] D. B. Reisman, et al., "The Advanced Helical Generator," Rev. Sci. Instrum. **81**, 034701 (2010).

[2] J. W. Shearer, et al., "Explosive-Driven Magnetic-Field Compression Generators," J. Appl. Phys. **39**, no. 4, pp. 2102-2116 (1968).

[3] D. B. Reisman, et al., "The Full Function Test Explosive Generator," Rev. Sci. Instrum. **81**, 036109 (2010).

[4] D. A. White, R. N. Rieben, B. K. Wallin, "Coupling Magnetic Fields and ALE Hydrodynamics for 3D Simulations of MFCG's," 2006 IEEE International Conference on Megagauss Magnetic Fields (2006).

[5] I. D. Smith, "Pulse Breakdown of Insulator Surfaces in Poor Vacuum," Proceedings of the International Symposium of High Voltages in Vacuum," Cambridge, MA, p. 261 (1964).

[6] W. A. Stygar, et al., "Improved Design of a High Voltage Vacuum-Insulator Interface," Phys. Rev. Special Topics – Accelerators and Beams, **8**, 050401 (2005).

[7] G. E. Vogtlin, W. W. Hofer, and M. J. Wilson, Lawrence Livermore National Laboratory UCRL Report No. 98704 (1988).

[8] G. E. Vogtlin and J. E. Vernazza, "Vacuum Insulator Failure Measurements and Improvement," Proceedings of the 7th IEEE Pulsed Power Conference, Monterey, CA, pp. 808-811 (1989).

[9] R. D. Scarpetti, D. A. Goerz, P. R. Bowen, R. L. Hodgin, K. C. Wong, and P. D'A. Champney, "Electron Emission from Conductors subjected to Intense Short-Pulse Electric Fields," Proceedings of the 6th IEEE International Pulsed Power Conference, Arlington, VA, p. 631 (1987).

[10] H. Oona, J. H. Goforth, D. G. Tasker, et al., "Studies of Plastic Insulators under Shock Conditions," Proceedings of the 28th IEEE Conference on Plasma Science / 13th IEEE International Pulsed Power Conference, Las Vegas, NV, pp. 1794-1797 (2001).

[11] O. Milton, "Pulsed Flashover of Insulators in Vacuum," IEEE Transactions on Electrical Insulation, Vol. **7**, No. 1 (1972).

[12] J. B. Javedani, D. A. Goerz, T. L. Houck, E. K. Lauer, R. D. Speer, L. K. Tully, G. E. Vogtlin, and A. D. White, "Understanding and Improving High Voltage Vacuum Insulators for Microsecond Pulses," LLNL LDRD Report UC-TR-228713 (2007).

[13] T. K. Tully, D. A. Goerz, T. L. Houck, and J. B. Javedani, "Electrostatic Modeling of Vacuum Insulator Triple Junctions," LLNL Report UCRL-TR-227505 (2006).

[14] M. P. Perkins, T. L. Houck, J. B. Javedani, G. E. Vogtlin, and D. A. Goerz, "Progress on Simulating the Initiation of Vacuum Insulator Flashover," Proceedings of the 17th IEEE International Pulsed Power Conference, Washington DC, pp. 441-446 (2009).

[15] M Wilson, D. A. Goerz, and R. D. Speer, "An Elegant Impulser Developed for Flat Beam Injection," Proceedings of the 23rd International Power Modulator Symposium, Rancho Mirage, CA, pp. 88-91 (1998).

[16] C. Enloe, R. Blaher, M. Coffing, R. E. Reinovsky, "Vacuum Ultra-Violet Effects on Power Transport Across A Vacuum/Solid Dielectric Interface," 10th International Symposium on Discharges and Electrical Insulation in Vacuum (1982).

[17] C. L. Enloe and R. E. Reinovsky, "Ultra-Violet Induced Insulator Flashover as a Function of Material Properties," Proceedings of the 4th IEEE Pulsed Power Conference, Albuquerque, NM, pp. 679-682 (1983).

[18] J. B. Javedani, T. L. Houck, B. T. Kelly, D. A. Lahowe, M. D. Shirk, and D. A. Goerz, "Ultra-Violet Induced Insulator Flashover," Proceedings of the 2008 IEEE International Power Modulator Conference, Las Vegas, NV, pp. 33-36.

[19] J. B. Javedani, T. L. Houck, D. H. Lahowe, G. E. Vogtlin, and D. A. Goerz, "Insulator Surface Flashover Due to UV Illumination," Proceedings of the 17th IEEE International Pulsed Power Conference, Washington DC, pp. 832-837 (2009).

[20] The ray-tracing code FRED is available from Photon Engineering, 440 South Williams Blvd., Suite 106, Tucson, AR, 85711, http://www.photonengr.com/.

[21] K. B. Bergeron and D. H. McDaniel, "Magnetic Inhibition in Vacuum," Appl. Phys. Let., **29** (9), pp. 543-536 (1976).

[22] J. P. VanDevender, D. H. McDaniel, E. L. Neau, R. E. Mattis, and K D. Bergeron, "Magnetic Inhibition of Insulator Flashover," J. Appl. Phys. **53** (6), pp. 4441-4447 (1982).